Evaluation of a Novel Wafer-Scale CMOS APS X-Ray Detector for Use in Mammography

Anastasios C. Konstantinidis, *Member, IEEE*, Yi Zheng, Alessandro Olivo, Kristina Bliznakova, Mary Yip, Thalis Anaxagoras, Kevin Wells, Nigel Allinson, and Robert D. Speller

***Abstract*–The most important factors that affect the image quality are contrast, spatial resolution and noise. These factors and their relationship are quantitatively described by the Contrast-to-Noise Ratio (CNR), Signal-to-Noise Ratio (SNR), Modulation Transfer Function (MTF), Noise Power Spectrum (NPS) and Detective Quantum Efficiency (DQE) parameters. The combination of SNR, MTF and NPS determines the DQE, which represents the ability to visualize object details of a certain size and contrast at a given dose. In this study the performance of a novel large area Complementary Metal-Oxide-Semiconductor (CMOS) Active Pixel Sensor (APS) X-ray detector, called DynAMITe (Dynamic range Adjustable for Medical Imaging Technology), was investigated and compared to other three digital mammography systems (namely a) Large Area Sensor (LAS), b) Hamamatsu C9732DK, and c) Anrad SMAM), in terms of physical characteristics and evaluation of the image quality. DynAMITe detector consists of two geometrically superimposed grids: a) 2560 x 2624 pixels at 50 μm pitch, named Sub-Pixels (SP camera) and b) 1280 x 1312 pixels at 100 μm pitch, named Pixels (P camera). The X-ray performance evaluation of DynAMITe SP detector demonstrated high DQE results (0.58 to 0.64 at 0.5 lp/mm). Image simulation based on the X-ray performance of the detectors was used to predict and compare the mammographic image quality using ideal software phantoms: a) one representing two three dimensional (3-D) breasts of various thickness and glandularity to estimate the CNR between simulated microcalcifications and the background, and b) the CDMAM 3.4 test tool for a contrast-detail analysis of small thickness and low contrast objects. The results show that DynAMITe SP detector results in high CNR and contrast-detail performance.**

I. INTRODUCTION

THIS study investigates the performance of a novel wafer-scale X-ray detector (named Dynamic Adjustable for Medical Imaging Technology - DynAMITe) based on Complementary Metal-Oxide-Semiconductor (CMOS) Active Pixel Sensor (APS) technology. We compare the objective X-ray performance (Signal Transfer Property (STP), Presampling Modulation Transfer Function (pMTF), Normalized Noise Power Spectrum (NNPS) and Detective Quantum Efficiency (DQE)) of DynAMITe to the respective of three mammographic detectors: a) Large Area Sensor (LAS; CMOS APS) [1], [2], b) Hamamatsu C9732DK (CMOS Passive Pixel Sensor (PPS)) [3] and c) Anrad SMAM (amorphous Selenium Thin Film Transistor (a-Se TFT)) [4].

Extracting information by the observer is the most important task in X-ray imaging. However, we can not easily predict the image quality from the objective X-ray performance evaluation because it does not involve the radiologists, radiographers or patients (i.e. subjective evaluation). Since image quality is task dependent we can not easily predict whether it is more strongly affected by the spatial resolution (pMTF) or the noise (NNPS) parameters [5]. To overcome this, the experimentally measured X-ray performance parameters were combined with ideal software phantoms to simulate images in mammographic conditions acquired with different X-ray detectors.

A modified version of Saunders and Samei [5] method was used [6], [7] to predict and compare the performance of the investigated detectors in digital mammography using ideal software phantoms: a) two three dimensional (3-D) breasts [8], [9] of different thickness (6 and 5 cm) and glandularity (45 and 73 %) to estimate the Contrast-to-Noise Ratio (CNR) between simulated microcalcifications (μCas) and the adjacent background, and b) the Artinis CDMAM 3.4 test tool [10] for a contrast-detail analysis of small thickness and low contrast objects [11]. The image quality evaluations were made for two Air Kerma levels at Detector surface (DAK): 59 and 120 μGy.

II. MATERIALS AND METHODS

A. DynAMITe CMOS APS X-ray detector

The Multidimensional Integrated Intelligent Imaging (MI-3) Plus consortium developed a novel large area three transistor (3-T) CMOS APS detector, named DynAMITe. The detector consists of two geometrically superimposed grids: a) fine-pitch grid diode (at 50 μm), named Sub-Pixels (SP camera), for low intrinsic noise and high spatial resolution and b) large-pitch grid diode (at 100 μm), named Pixels (P camera), for high dynamic range, i.e. 1280 x 1312 Pixels and 2560 x 2624 Sub-Pixels (resulting in 12.8 cm x 13.1 cm active area) [12]. The diodes of the two arrays are reset at different voltages to control the different depletion widths of each diode, i.e. we

Manuscript received November 14, 2012. This work was supported by the EPSRC Multidimensional Integrated Intelligent Imaging Plus (MI-3 Plus) programme (EP/G037671/2).

A. C. Konstantinidis, Y. Zheng, A. Olivo, and R. D. Speller are with the Department of Medical Physics and Bioengineering, University College London, London WC1E 6BT, U.K. (e-mail: anastasios.konstantinidis@ucl.ac.uk).

K. Bliznakova is with the Department of Electronic Engineering and Microelectronics, Technical University of Varna, Varna, 9010, Bulgaria (e-mail: kristina.bliznakova@gmail.com).

M. Yip and Kevin Wells are with the Center for Vision, Speech and Signal Processing, Faculty of Engineering and Physical Sciences, University of Surrey, Guildford, GU2 7XH, U.K. (e-mail: k.wells@surrey.ac.uk).

T. Anaxagoras is with the ISDI Ltd (Image Sensor Design and Innovation), Oxford, OX4 1YZ, U.K. (e-mail: t_anaxagoras@hotmail.com).

T. Anaxagoras and N. Allinson are with the Image Engineering Laboratory, University of Lincoln, Lincoln, LN6 7TS, U.K. (e-mail: nallinson11@gmail.com).

can use 50, 100 µm resolution or their combination. In this study we used the SP camera only to compare its X-ray performance to the respective of the other mammographic detectors [6]. A structured Thallium-activated Caesium Iodide (CsI:Tl) scintillator (150 µm thick) was coupled to DynAMITe to constitute the X-ray detector.

B. Image Simulation Based on the X-ray Performance Evaluation

The DQE expresses the ability of an X-ray detector to transfer the Signal-to-Noise Ratio (SNR) from its input to the output. It expresses the fraction of input X-ray photons used to create an image at each spatial frequency and describes the ability of a particular system to effectively use the available input quanta:

$$DQE(f) = \frac{SNR_{out}^2}{SNR_{in}^2} = \frac{pMTF^2(f)}{\Phi \cdot NNPS(f)} \quad (1)$$

where Φ is the photon fluence (expressing the SNR^2 input in X-rays/mm^2). The measurements and calculations of pMTF, NNPS and DQE were made at 28 kV using Tungsten/Aluminum (W/Al) anode/filtration combination, which is one of the eight radiation beam qualities proposed by the mammographic IEC standard [13].

Fig. 1 presents the flowchart of the implementation of the signal and noise transfer on ideal images to get the synthetic radiographic images. Briefly, the two dimensional (2-D) pMTF matrix of a digital X-ray detector is multiplied with an ideal input image in the frequency domain to insert blurring. Then an inverse Fourier transform is applied on the product and the blurred image is sampled to form the pixels of the digital image. The measured NNPS distribution is used to create a flat image with noise. This noise image is rescaled at specific DAK level and added to the blurred and sampled object image to form the final simulated image. Further details can be found in [5]–[7].

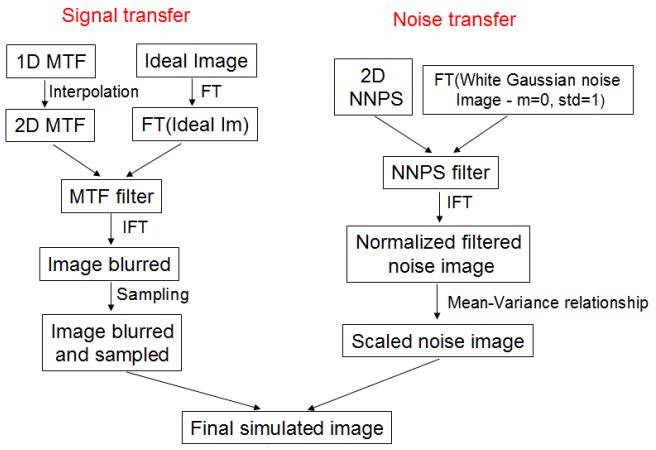

Fig. 1. Image simulation algorithm flowchart [6].

C. Image Quality Evaluation

Two breast software phantoms at different composition (45 and 73 % glandularity) and thickness (6 and 5 cm, respectively) were used as ideal input images based on [8], [9]. Briefly, the ideal software phantoms are 2-D X-ray projection images (at craniocaudal (CC) orientation) of compressed 3-D software breasts containing the breast external shape, skin, mammary duct system, breast abnormalities, mammographic texture, Cooper's ligaments, pectoralis muscle, lymphs, and blood vessels. Both breast phantoms contained $CaCO_3$ spheres with 0.6 mm diameter to simulate µCas. The 3-D breast models were reconstructed as 2-D projection images at a given angle θ to generate a set of line integrals with 10 µm "analog" pitch. Further details about this can be found in [6].

Table I shows the main parameters related to the ideal software breast phantoms. It should be noted that the synthetic mammograms correspond to two distinct DAK levels: 59 and 120 µGy. We selected the first one because LAS saturates when DAK is higher than 60 µGy. The second one is within the average mammographic DAK range (100-120 µGy) normally found in the literature [6].

TABLE I. PARAMETERS RELATED TO THE SYNTHETIC BREAST PHANTOMS

Parameter	Breast 1	Breast 2	Unit
Thickness	5	6	(cm)
Granularity	73	45	(%)
µCa diamet.	0.6	0.6	(mm)
DAK 1	59	59	(µGy)
DAK 2	120	120	(µGy)

Fig. 2 shows the synthetic mammogram of Breast 2 using DynAMITe SP detector (at 120 µGy DAK). To implement the CNR analysis, circular regions of interest (ROIs) were extracted from the center of each 2-D $CaCO_3$ disk image. The size of the ROI was taken in order to be in the central area of the disk (i.e. the diameters of the ROIs were from 0.4 to 0.5 mm). Then, four circular ROIs were selected from adjacent background areas with diameter three times larger than that of the disk ROI (i.e. from 1.2 to 1.5 mm). Both the number and size of the background ROIs were selected to take into account the variations of the background.

The CNR was calculated using the following formula:

$$CNR = \frac{m_o - m_b}{\sqrt{\frac{\sigma_o^2 + \sigma_b^2}{2}}} \quad (2)$$

where m_o is the average digital number (DN) of the object (i.e. $CaCO_3$), m_b is the average DN of the background, σ_o is the average standard deviation of the object, and σ_b is the average standard deviation of the background.

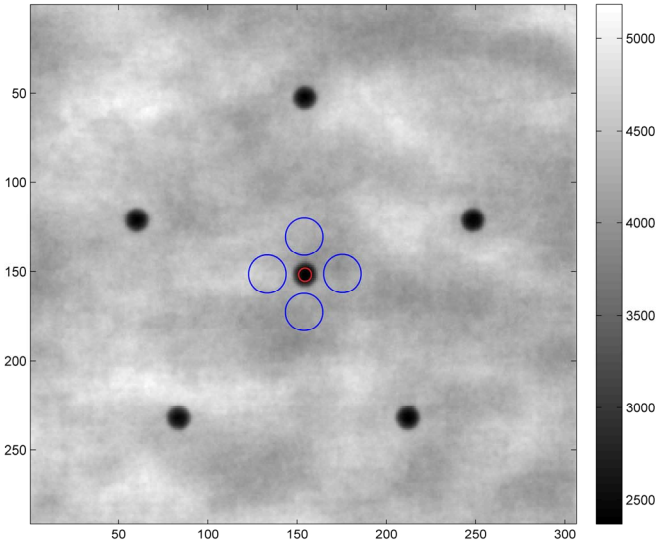

Fig. 2. Synthetic mammogram at 120 μGy DAK (Breast 2) using DynAMITe SP detector.

According to the European Guidelines for quality control in digital mammography, the mammographic image quality is expressed in terms of threshold contrast visibility using clinical exposure settings [11], [14]. The threshold contrast is defined as the lowest contrast value for which the objects are visible. In this study a slightly modified version (0.3 mm instead of 0.5 mm Al to simulate 50 mm PMMA in total - see [6]) of the Artinis CDMAM 3.4 test tool [10] was used to compare the ability of the investigated digital systems to detect very low contrast and very small details (contrast-detail analysis). The used software phantom consists of a 16 cm x 24 cm x 0.3 mm Al plate with 205 square cells (arranged in 16 rows x 16 columns). Each cell contains two identical gold disks (one at the center and one in a randomly chosen corner - eccentric disk) of given thickness and diameter that decrease logarithmically to cover a range of object diameters from 2.00 to 0.06 mm in each column and thicknesses between 2.00 and 0.03 mm in each row. The CDMAM phantom is used to determine the contrast limit (threshold contrast) or threshold gold thickness for a given disk diameter that corresponds to successful observation of the eccentric disk location. Fig. 3 shows the synthetic radiograph of CDMAM 3.4 test tool using DynAMITe detector (at 120 μGy DAK). It should be noted that scatter and geometrical blurring were taken into account (scatter to primary radiation ratio equal to 0.62, magnification factor equal to 1.08 and focal spot equal to 300 μm [6]).

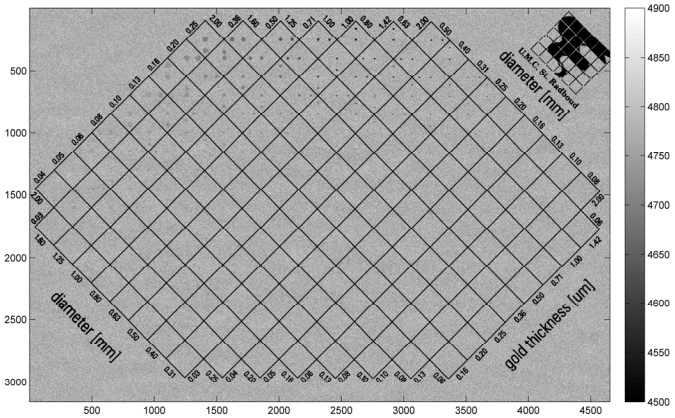

Fig. 3. Synthetic radiograph of CDMAM 3.4 test tool at 120 μGy DAK using DynAMITe SP detector.

The evaluation of the CDMAM 3.4 test tool radiographs was made using the freeware CDCOM 1.5.2 software tool [15], which provides the detected eccentric and center disks. Further analysis, based on the psychometric curve fit [16], was made to calculate the threshold thickness for a given diameter:

$$p(t) = \frac{0.75}{1 + e^{-f\left(\frac{t}{t_T}\right)}} + 0.25 \qquad (3)$$

where $p(t)$ is the probability to detect a disk, t is the disk thickness (in μm), t_T is the threshold thickness (i.e. the thickness that corresponds to p(t)=0.625) and f is a free parameter to be fitted.

A custom built Graphical User Interface (GUI) was developed in MATLAB (named *CDMAM_fit_2*) throughout this study to apply psychometric curve fitting based on [11]. Briefly, the *CDMAM_fit_2* reads the CDCOM output data. Then, it converts the original CDCOM data to a probability matrix, applies edge padding and smoothes the probability data (via convolution) using a Gaussian (3 x 3 mask with σ=1) filter [17]. Next, we can apply psychometric curve fit (3) and predict the human readout threshold thickness by applying a power function [18]. The resultant data are fitted (in semi-logarithmic scale) with a third order polynomial function to obtain the contrast-detail curve [19]. Finally, the software gives the option to save the predicted results in various formats (txt, csv and Excel). Fig. 4 shows two screenshots of the *CDMAM_fit_2* GUI.

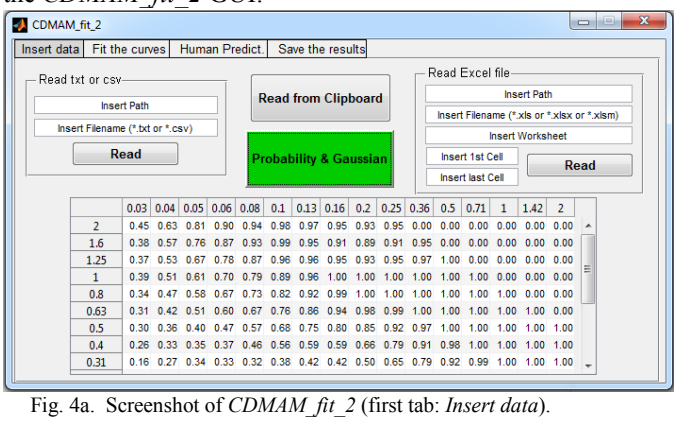

Fig. 4a. Screenshot of *CDMAM_fit_2* (first tab: *Insert data*).

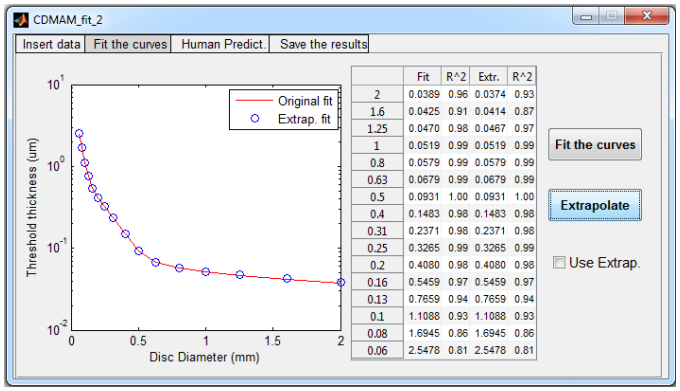

Fig. 4b. Screenshot of *CDMAM_fit_2* (second tab: *Fit the curves*).

III. RESULTS AND DISCUSSION

A. X-ray Performance Evaluation of the detectors

Fig. 5 shows the STP curves with linear fitting function equations for LAS, Hamamatsu, DynAMITe SP and Anrad SMAM detectors at 28 kV (W/Al). It should be noted that the STP curve gives information about the sensitivity and linearity of the signal transfer of X-ray detectors. Both LAS and DynAMITe SP show relatively high sensitivity to the incident x-ray photons. In particular, LAS saturates for DAK higher than 60 µGy. All X-ray detectors show sufficient linearity in the signal transfer with R^2 greater than 0.997.

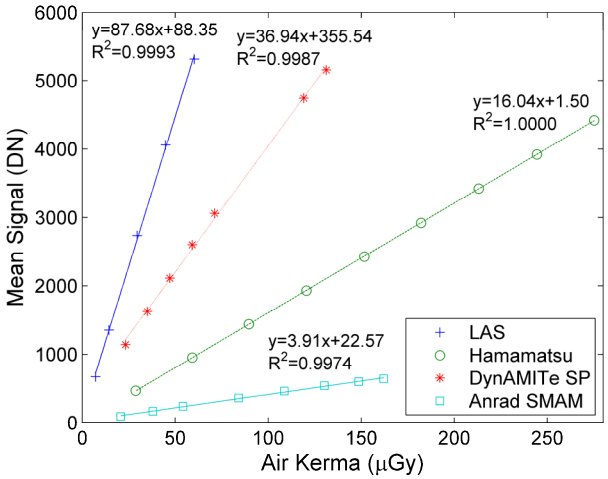

Fig. 5. STP curves of the investigated detectors at 28 kV (W/Al).

Fig. 6 shows the average pMTF values of the investigated detectors. The high average pMTF value of Anrad SMAM (around 0.53) at Nyquist frequency (F_{Nyq}) suggests significant aliasing contribution from higher frequencies, which is a common effect on direct conversion detectors. Hamamatsu and DynAMITe SP have similar MTF values due to the same pixel pitch and similar thickness of CsI:Tl scintillator (160 versus 150 µm). LAS has very low pMTF values due to unoptimized usage of the optical coupling gel between the fibre optic plate (FOP) and the detector surface [6].

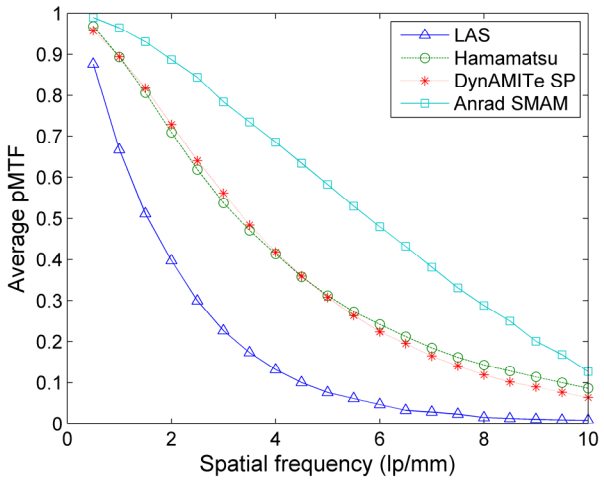

Fig. 6. Average pMTF curves of the X-ray detectors at 28 kV (W/Al).

Fig. 7 shows the average DQE curves of LAS in the DAK range 7.2-60.3 µGy. LAS presents high DQE values at low spatial frequencies (the DQE at 0.5 line pairs per mm (lp/mm), i.e. DQE(0.5), is in the range 0.61-0.73), and lower ones at medium frequencies (> 4.5 lp/mm). LAS DQE curves do not present quantum limited behavior, i.e. they do not overlap at high DAK levels, probably due to the inherent V/e^- nonlinearity of CMOS APS sensors [6].

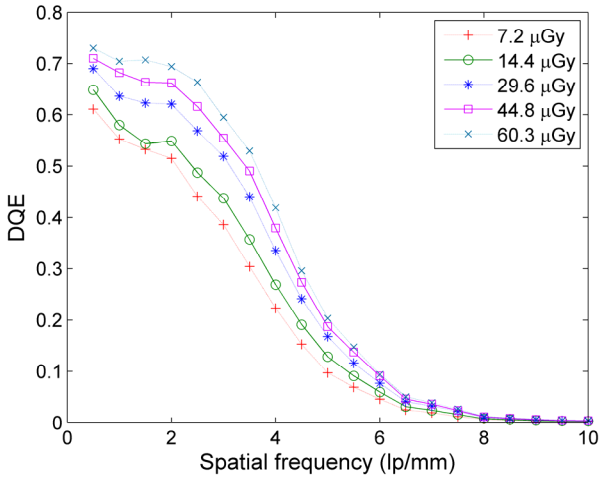

Fig. 7. Average DQE curves of LAS at 28 kV (W/Al).

Fig. 8 shows the average DQE curves of Hamamatsu C9732DK in the DAK range 28.7-275.2 µGy. This detector presents a quantum limited performance over a broad exposure range (e.g. the DQE(1) is in the range 0.45-0.47). This is related to the linear STP and SNR transfer of the detector. A small drop of DQE curves is observed at 0.5 lp/mm, probably due to remnant low-frequency trends that affect the NNPS calculation. The DQE curve of the lowest DAK level (28.7 µGy) is slightly lower, probably due to the high read noise (1250 e^- root mean square (r.m.s.) nominal level) of the detector.

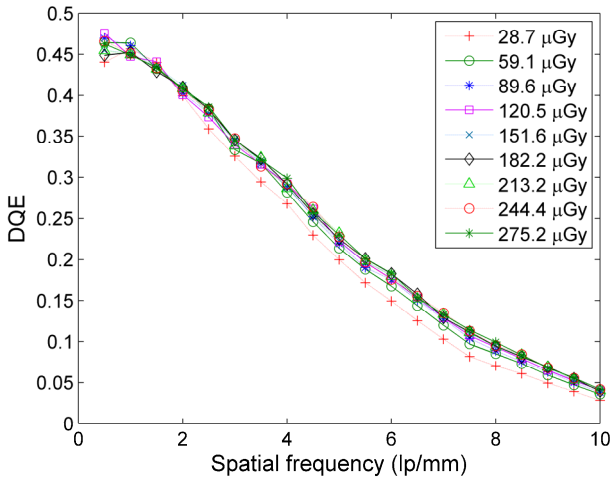

Fig. 8. Average DQE curves of Hamamatsu C9732DK detector at 28 kV (W/Al).

Fig. 9 shows the average DQE curves of DynAMITe SP in the DAK range 23.3-131.2 µGy. It demonstrates good X-ray detectability at low spatial frequencies (the DQE(0.5) is in the range 0.58-0.64)

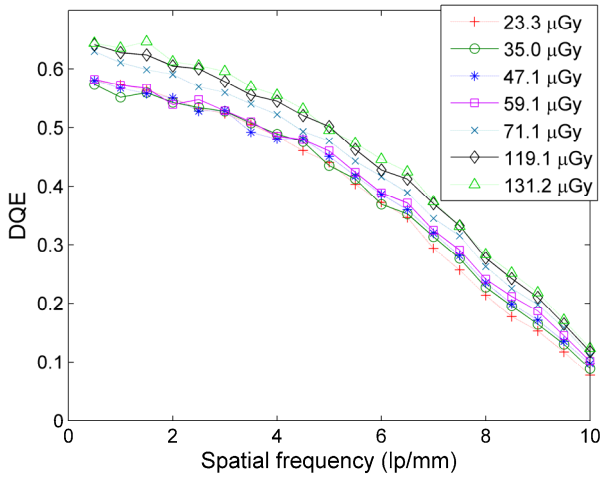

Fig. 9. Average DQE curves of DynAMITe SP detector at 28 kV (W/Al).

Finally, Fig. 10 shows the average DQE values of Anrad SMAM in the DAK range 20.7-162.1 µGy. This detector demonstrates lower DQE values at low DAK levels (20.7 and 38.0 µGy), probably due to the strong effect of the read noise (5200 e^- r.m.s [6]). However, at high DAK levels (84.1-162.1 µGy) the DQE curves are overlapped, demonstrating a quantum limited behavior. In particular, the DQE(0.5) at high DAK levels is in the range 0.64-0.67.

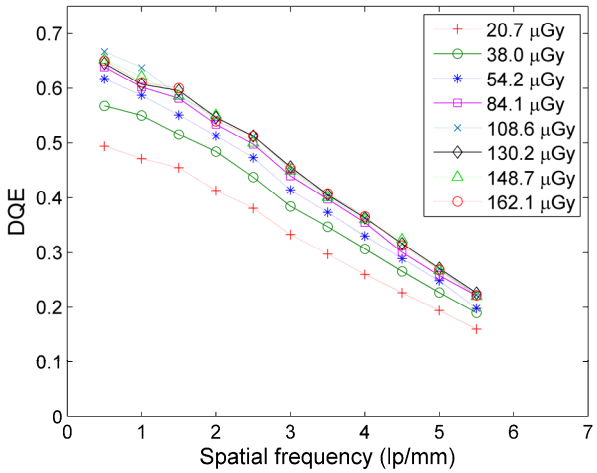

Fig. 10. Average DQE curves of Anrad SMAM detector at 28 kV (W/Al).

To summarize, Hamamatsu, DynAMITe SP and Anrad SMAM detectors demonstrate quantum limited behavior at higher DAK levels. Also, LAS, DynAMITe SP and Anrad SMAM detectors show high DQE values at low spatial frequencies.

B. Image Quality Evaluation of the Simulated Images

Fig. 11 shows the CNR curves of the investigated detectors for the synthetic Breast 1 (5 cm and 73 % glandularity) for both 59 and 120 µGy DAK. It can be observed that LAS and DynAMITe SP detectors present the highest visibility of µCas with relatively high diameter (600 µm). The CNR values are higher at 120 µGy because higher exposure corresponds to higher number of X-rays, which are information carriers, and the noise effect decreases.

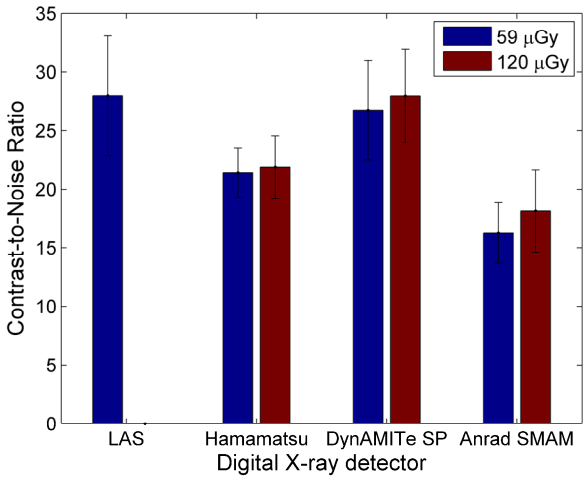

Fig. 11. CNR curves for the synthetic Breast 1 (59 and 120 µGy).

Fig. 12 demonstrates the CNR curves of the investigated detectors for the synthetic Breast 2 (6 cm and 45 % glandularity). Again, we can see that LAS and DynAMITe SP detectors result in the highest CNR values.

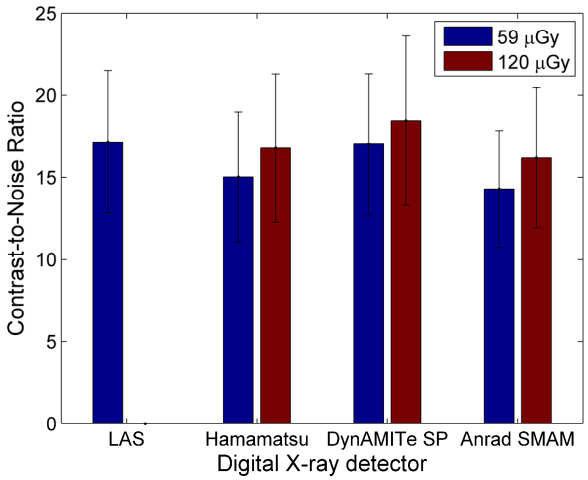

Fig. 12. CNR curves for the synthetic Breast 2 (59 and 120 μGy).

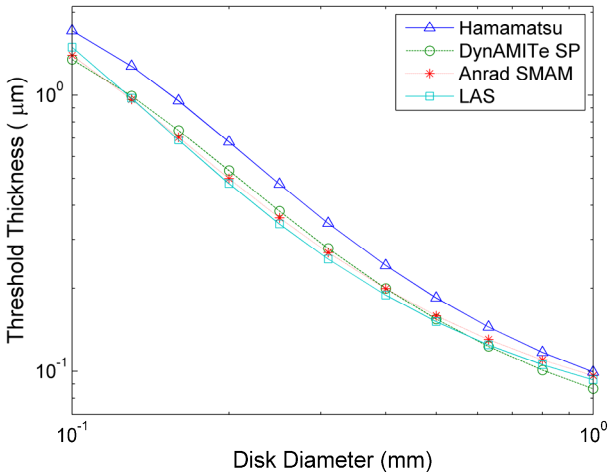

Fig. 13. Threshold thickness as a function of disk diameter at 59 μGy.

It should be noted that direct comparison of different systems using CNR can be problematic. Comparing two systems (e.g. A and B), it is possible for system A to have higher CNR than B but for B to have a better (i.e. lower) low contrast detectability result. Therefore, there is no universal target CNR or SDNR used as a minimum image quality standard for all systems. Furthermore, this comparison depends mainly on the SNR transfer of each detector due to the relatively large dimensions of the simulated microcalcifications (600 μm diameter). It does not fully examine the effect of the detector's signal transfer at different frequencies. Hence, we also compare the performance of the detectors using the CDMAM 3.4 test tool.

Fig. 13 presents the threshold thickness curves of the investigated detectors as a function of disk diameter at 59 μGy DAK. All of them were extracted by combining 8 CDMAM 3.4 images per detector. For clarity we do not present the uncertainty on the graph (less than 10 % in all cases), which is expressed by the 95 % confidence level on the nonlinear least mean squares psychometric curve fit using *CDMAM_fit_2*. It may be observed that Hamamatsu detector has the highest threshold thickness values at all disc diameters, which corresponds to the lowest performance because we need thicker disks to get p(t)=0.625. On the other hand, LAS, DynAMITe SP and Anrad SMAM detectors demonstrate similar performance at almost all disk diameters.

Fig. 14 demonstrates the threshold thickness curves of Hamamatsu, DynAMITe SP and Anrad SMAM detectors at 120 μGy DAK. Again, Hamamatsu C9732DK detector has the lowest performance in all disk diameters (probably because of the relatively low DQE results). On the other hand, DynAMITe SP and Anrad SMAM have similar performance at almost all disk diameters. It is observed that Anrad has lower performance than DynAMITe SP at low disk diameters (i.e. 0.1-0.16 mm) despite its high pMTF values (Fig. 6). This happens due to the aliasing effect that increases the NNPS and consequently decreases the DQE at higher spatial frequencies (Fig. 10).

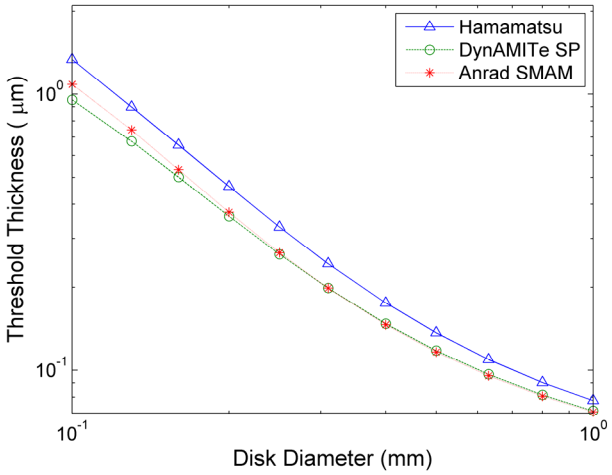

Fig. 14. Threshold thickness as a function of disk diameter at 120 μGy.

IV. CONCLUSIONS AND FUTURE WORK

DynAMITe SP detector presents high X-ray sensitivity, MTF and DQE values compared to the other three detectors. Image simulation based on the X-ray performance evaluation was used to predict that DynAMITe exhibits high CNR values for 0.6 mm diameter μCas in thick (5 and 6 cm) and high glandularity (73 %) breasts. Finally, it has high contrast-detail performance, especially for small disk diameters (0.1-0.2 mm)

and 120 μGy DAK. From the above results we conclude that DynAMITe SP detector is suitable for use in Mammography. More suitable mammographic anode/filtration combinations (such as Molybdenum (Mo) anode with Mo filtration (Mo/Mo)) may result in better DQE results / image quality. Finally, non-uniformity effects (such as heel-effect, local pixel variance and non-uniform scatter model derived with Monte Carlo) can be taken into account to generate more clinically realistic CDMAM 3.4 images [20].

ACKNOWLEDGMENT

Special thanks go to the OPTIMAM project for providing the software CDMAM 3.4 test tool.

REFERENCES

[1] N. Allinson et al., "The Multidimensional Integrated Intelligent Imaging project (MI-3)," Nucl. Instr. Meth. A, vol. 604, pp. 196-198, 2009.

[2] S. E. Bohndiek et al., "Characterization and testing of LAS: A prototype "Large Area Sensor" with performance characteristics suitable for medical imaging applications," IEEE Trans. Nucl. Sc., vol. 56, pp. 2938-2946, 2009.

[3] Hamamatsu, Flat panel sensor C9732DK: For soft X-ray imaging, cassette type with USB 2.0 interface. Large photodiode area: 120 x 120 mm, 2008.

[4] Anrad, The SMAM digital detector, digital mammography applications – product information, 2004.

[5] R. S. Saunders and E. Samei, "A method for modifying the image quality parameters of digital radiographic images," Med. Phys., vol. 30, pp. 3006-3017, 2003.

[6] A. C. Konstantinidis, "Evaluation of digital X-ray detectors for medical imaging applications," Ph.D. thesis, Dept. Medical Physics and Bioengineering, University College London, London, UK, 2011.

[7] A. C. Konstantinidis, A. Olivo, and R. D. Speller, "Technical Note: Further development of a resolution modification routine for the simulation of the modulation transfer function (MTF) of digital X-ray detectors," Med. Phys., vol. 38, pp. 5916-5920, 2011.

[8] K. Bliznakova, S. Suryanarayanan, A. Karellas, and N. Pallikarakis, "Evaluation of an improved algorithm for producing realistic 3D breast software phantoms: Application for mammography," Med. Phys.,vol. 37, pp. 5604-5617, 2010.

[9] K. Bliznakova, I. Sechopoulos, I. Buliev, and N. Pallikarakis, "BreastSimulator: A software platform for breast x-ray imaging research," J. Biomed. Graph. Comput., vol. 2, pp. 1-14, 2012.

[10] M. Yip et al., "Validation of a digital mammography image simulation chain with automated scoring of CDMAM images," Proc. IWDM 2008: Lect. Not. Comp. Sci., vol. 5116, pp. 409-416, 2008.

[11] K. C. Young et al., "Comparison of software and human observers in reading images of the CDMAM test object to assess digital mammography systems," Proc. SPIE, vol. 6142, 14206-1, 2006.

[12] M. Esposito et al., "DynAMITe: a wafer scale sensor for biomedical applications," Journ. Instr., vol. 6, C12064, 2011.

[13] IEC 62220-1-2, Medical electrical equipment-characteristics of digital X-ray imaging devices: Part 1–2. Determination of the detective quantum efficiency-detectors used in mammography, International Electrotechnical Commission (IEC), Geneva, Switzerland, 2007.

[14] R. E. van Engen, K. C. Young, H. Bosmans, and M. A. O. Thijssen, "European protocol for the quality control of the physical and technical aspects of mammography screening. Part B: Digital mammography" in *European guidelines for quality assurance in breast cancer screening and diagnosis*, 4th ed., Luxembourg: European Commission, 2006, ch. 2a, pp. 105-165.

[15] R. Visser and N. Karssemeijer, Manual CDCOM version 1.5.2: software for automated readout of CDMAM 3.4 images, 2008.

[16] N. Karssemeijer and M. A. O. Thijssen, "Determination of contrast-detail curves of mammography systems by automated image analysis," Proc. IWDM, vol. 1119, pp. 155-160, 1996.

[17] B. Verbrugge, "Validation of analysis methods for automated CDMAM reading," B.A. thesis, Department of Physics and Astronomy in collaboration with the Department of Medical Diagnostic Science, Katholieke Universiteit Leuven, Belgium, 2007.

[18] K. C. Young et al., "Evaluation of software for reading images of the CDMAM test object to assess digital mammography systems," Proc. SPIE, vol. 6913, C9131-1, 2008.

[19] R. E. van Engen et al., "A supplement to the European Guidelines for Quality Assurance in Breast Cancer Screening and Diagnosis," Proc. IWDM 2010: Lect. Not. Comp. Sci., vol. 6136, pp. 643–650, 2010.

[20] M. Yip, "Image Simulation Framework for Digital Mammography Systems," Ph.D. thesis, Centre for Vision, Speech and Signal Processing, University of Surrey, Guilford, UK, 2010.